Journal Name

ARTICLE

Mitochondria-localising DNA-binding biscyclometalated phenyltriazole iridium(III) dipyridophenazene complexes: syntheses and cellular imaging properties

Received 00th January 20xx,
Accepted 00th January 20xx

DOI: 10.1039/x0xx00000x

www.rsc.org/

Sreejesh Sreedharan,[c]† Alessandro Sinopoli,[a,b]† Paul. J. Jarman,[d] Darren Robinson,[d] Christopher Clemmet,[a] Paul A. Scattergood,[a] Craig R. Rice,[a] Carl. G. W. Smythe,[d] James A. Thomas[c]* and Paul I.P. Elliott[a]*

Two new biscyclometalated complexes $[Ir(ptz^R)_2(dppz)]^+$ (dppz = dipyridophenazene; ptz^RH = 4-phenyl-1-benzyl-1,2,3-triazole (**1**$^+$) and 4-phenyl-1-propyl-1,2,3-triazole (**2**$^+$)) have been prepared. The hexafluorophosphate salts of these complexes have been fully characterized and, in one case, the X-ray structure of a nitrate salt was obtained. The DNA binding properties of the chloride salts of the complexes were investigated, as well as their cellular uptake by A2780 and MCF7 cell lines. Both complexes display an increase in the intensity of phosphorescence upon titration with duplex DNA, indicating the intercalation of the dppz ligand and, given that they are monocations, the complexes exhibit appreciable DNA binding affinity. Optical microscopy studies reveal that both complexes are taken up by live cancer cell lines displaying cytosol based luminescence. Colocalization studies with commercial probes show high Pearson coefficients with mitotracker dyes confirming that the new complexes specifically localize on mitochondria.

Introduction

Phosphorescent complexes of kinetically inert d^6 metals such as rhenium(I), ruthenium(II) and iridium(III) have become increasingly attractive for the development of novel luminescent cellular imaging agents for confocal microscopy.[1-7] Luminescent complexes of this type offer several advantages over purely organic luminophores; the ability to readily access phosphorescent triplet states results in longer lifetimes of emission, enabling their use in time-gated imaging applications which removes unwanted background autofluorescence deriving from biological materials.[8, 9] Further, the structures of the ligands in these complexes can be readily modified to; tune the photophysical properties, augment the balance between lipophilicity and hydrophilicity to maximize cellular uptake, and can be derivatised to facilitate organelle targeting.[2]

One the most studied examples of emissive transition metal complexes in this area is the DNA "light switch", $[Ru(N^N)_2(dppz)]^{2+}$ (N^N = 2,2'-bipyridyl, phenanthroline, Chart 1).[10-12] When this complex interacts with DNA, the extended planar dppz ligand intercalates between base pairs of the duplex. A consequence of this interaction is that water molecules are excluded from hydrogen bonding with N-donor sites of dppz, "switching on" the Ru→dppz-based ^{3}MLCT emission of the complex.

Iridium complexes have also been actively targeted for their use in biological imaging and diagnostics,[13-17] and developed as imaging probes for specific organelles, including mitochondria.[18-26] Biscyclometalated iridium(III) complexes bearing dppz-like ligands have also been investigated.[27-33] Although these systems often display lower DNA binding constants compared to their dicationic Ru^{II} analogues due to the reduced electrostatic attraction between the monocationic complex and the anionic phosphates of the DNA polymer backbone, the increased stability of iridium(III) complexes to ligand-loss and the high degree of stereochemical control of the coordination environment in these complexes offers some significant advantages in the development of DNA-targeting systems. Furthermore, given that cellular uptake is often closely related to increased hydrophobicity, the lower charge of such species may actually be advantageous for cell imaging applications. With this in mind, we pursued the synthesis and characterization of two new complexes, each bearing a dppz intercalating ligand along with phenyltriazole-based cyclometalated ligands (Chart 1).

[a] Department of Chemistry, University of Huddersfield, Queensgate, Huddersfield, HD1 3DH, UK.
[b] Qatar Environmental & Energy Research Institute, Hamed Bin Khalifa University, PO Box 5825, Doha, Qatar.
[c] Department of Chemistry, University of Sheffield, Western Bank, Sheffield, S3 7HF, UK.
[d] Department of Biomedical Science, University of Sheffield, Western Bank, Sheffield, S3 7HF, UK.
* corresponding authors: james.thomas@sheffield.ac.uk; p.i.elliott@hud.ac.uk
† These authors contributed equally to the work.
Electronic Supplementary Information (ESI) available: [details of any supplementary information available should be included here]. See DOI: 10.1039/x0xx00000x

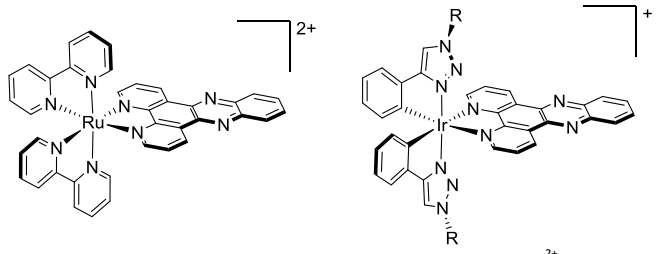

Chart 1. Structures of DNA "light switch" complex $[Ru(bpy)(dppz)]^{2+}$ (left) and the prototypical iridium(III) intercalator complex $[Ir(ptz^{R})_2(dppz)]^{+}$ reported here (right).

Triazole-based compounds have become popular ligand motifs in coordination chemistry and photophysics.[34-36] Since stereoselectivity in synthesis would place the triazole rings *trans* to one another and *cis* to the dppz ligand, we anticipated that the N2 atoms of these rings would point towards the DNA upon intercalation. We reasoned that this might lead to stabilization of a resultant DNA adduct through additional H-bonding interactions with sugar O-H or base N-H protons. Axially positioned triazole substituents (R) could also potentially provide additional H-bonding or π-stacking moieties. Consequently, to investigate these possibilities, our two prototype complexes either include benzyl substituents as potential additional intercalating groups, or simple propyl chains where such interactions are not possible.

In this paper we present our preliminary results on the synthesis and characterization of these complexes as well as the investigation of their DNA binding properties and cellular uptake, localisation and luminescence imaging studies.

Results and Discussion

Synthesis and characterisation.

The biscyclometalated complexes $\mathbf{1}^+$ and $\mathbf{2}^+$ were prepared using the two-step procedure shown in Scheme 1. Iridium(III) chloride and the corresponding 4-phenyl-1,2,3-triazole ligand precursor were combined in ethoxyethanol/water (3:1), heated to reflux for twelve hours, and then allowed to cool to room temperature. The crude dimers were then reacted with dppz in refluxing dichloromethane/methanol and the product was purified by column chromatography using acetonitrile/saturated aqueous KNO_3 and ultimately isolated as their hexafluorophosphate salts.

Complexes $\mathbf{1}^+$ and $\mathbf{2}^+$ have been fully characterised using ^1H and ^{13}C NMR spectroscopy, and mass spectrometry. The ^1H NMR spectra of $\mathbf{1}^+$ and $\mathbf{2}^+$ exhibit a single set of resonances for the cyclometalated ligands along with five resonances for the dppz ligand as a consequence of the C_2 symmetry of the complexes. The resonances for the triazole protons of $\mathbf{1}^+$ and $\mathbf{2}^+$ appear at δ 8.15 and 8.40 respectively and are deshielded by approximately 0.5 to 0.6 ppm relative to their phenyltriazole free ligand precursors.

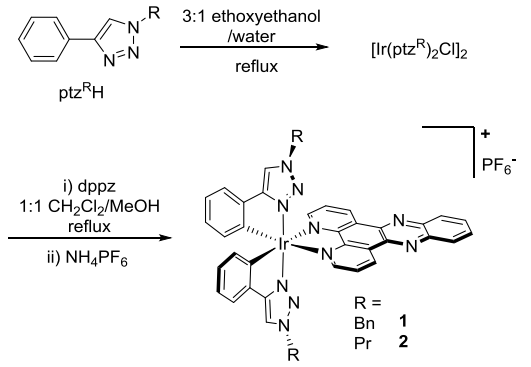

Scheme 1. Synthetic route to complexes **1**.PF_6 and **2**.PF_6.

Several unsuccessful attempts were made to obtain X-ray diffraction quality crystals of the complexes as hexafluorophosphate salts. However, suitable crystals were obtained for $\mathbf{1}^+$ as its nitrate salt $[Ir(ptz^{Bn})_2(dppz)][NO_3].2.5CH_2Cl_2$. from dichloromethane layered with hexane. The structure of the cation $\mathbf{1}^+$ is shown in Figure 1. The complex crystallised in the space group P21/n with two cations per unit cell. The cation adopts the expected distorted octahedral geometry for a heteroleptic biscyclometalated iridium(III) complex in which the two triazole N-donors are situated mutually *trans* to one another with the aryl rings in a *cis* arrangement. The metal-ligand bond lengths in the complex are unremarkable with Ir-N distances varying from 2.000(5) to 2.145(4) Å, with those for the cyclometalated ligand being slightly shorter than those to dppz. The bite angles of the cyclometalating ligands are 79.3(2) and 79.6(2) ° with that for the dppz ligand being slightly narrower at 77.23(18) °.

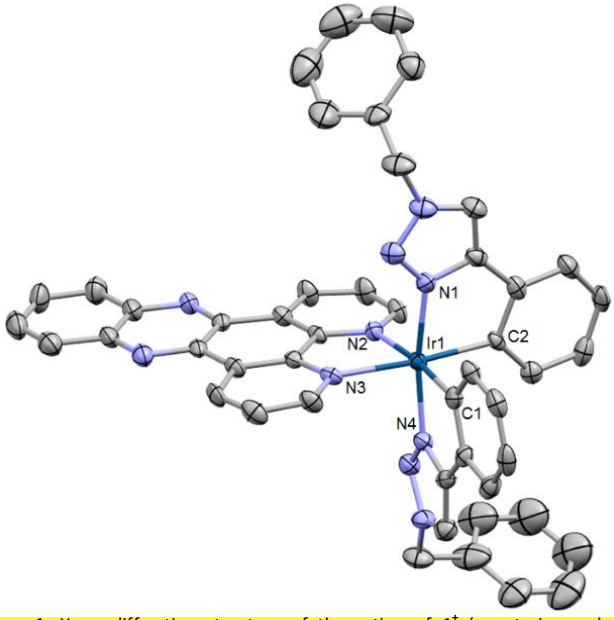

Figure 1. X-ray diffraction structure of the cation of $\mathbf{1}^+$ (counterion, solvent molecules and hydrogen atoms removed for clarity. Ellipsoids at 50 % probability). Selected bond lengths (Å) and angles (°): Ir1-N1 2.023(5); Ir1-N2 2.145(4); Ir1-N3 2.137(5); Ir1-N4 2.000(5); Ir1 C1 2.049(6); Ir1 C2 2.029(6); N1-Ir1-C2 79.3(2); N4-Ir1-C1 79.6(2); N3-Ir1-N2 77.23(18); N4-Ir1-N1 170.0(2); C2-Ir1-N3 173.2(2); C1-Ir1-N2 173.5(2).

Table 1. Photophysical properties of complexes as their chloride salts.

Complex	λ^{abs} / nm [a]	λ^{em} / nm [a,b]	τ / ns [a,b]	τ / ns [a,c]	ϕ / % [a,b,d]	ϕ / % [a,c,d]
1$^+$	442 (1100), 385 (8500), 364 (10100), 276 (54660)	672	τ_1 = 23 (12 %) τ_2 = 57 (78 %) τ_3 = 268 (10 %)	τ_1 = 43 (27 %) τ_2 = 92 (42 %) τ_3 = 1118 (31 %)	0.12	0.21
2$^+$	442 (1125), 385 (7200), 365 (8180), 276 (42300)	675	τ_1 = 40 (56 %) τ_2 = 101 (22 %) τ_3 = 335 (22 %)	τ_1 = 57 (9 %) τ_2 = 275 (14 %) τ_3 = 1117 (77 %)	0.08	0.43

[a] recorded in acetonitrile. [b] aerated solutions at RT, [c] deaerated solutions at RT, [d] ϕ_p for $[Ru(bpy)_3(PF_6)_2]$ 0.018 (air).

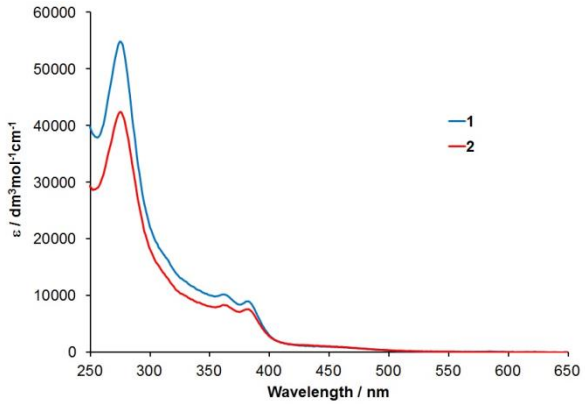

Figure 2 UV-visible absorption spectra of **1**$^+$ and **2**$^+$ complexes as their chloride salts in acetonitrile.

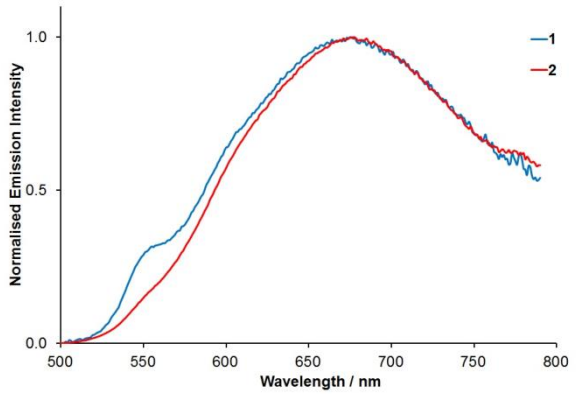

Figure 3 Emission spectra of complexes **1**$^+$ and **2**$^+$ as their chloride salts in acetonitrile.

In order to improve aqueous solubility for subsequent biological studies the hexafluorophosphate salts **1**.PF_6 and **2**.PF_6 were subject to anion metathesis to yield their chloride salts **1**.Cl and **2**.Cl.

UV-Visible absorption spectra of both complexes as their chloride salts were recorded in aerated acetonitrile solutions at room temperature (Figure 2). Both complexes show intense bands in the ultraviolet region at 280 nm attributed to spin-allowed π-π* ligand-centred (^{1}LC) transitions. This assignment was made on assessment of closely related metal complexes in the literature.[37] The less intense, lower energy absorption features from 300 to 420 nm are due to ^{1}MLCT/LLCT charge-transfer (CT) transitions. However, these are coincident with further absorption bands associated with the dppz ligand and will thus have additional ^{1}LC contributions in this region. Absorptions of much weaker intensity between 400 and 500 nm are assigned as arising from transitions having spin-forbidden ^{3}MLCT character.[38] Due to the minimal effect of the triazole N1 substituents on the photophysical properties of **1**$^+$ and **2**$^+$ the absorption spectra of the two complexes are nearly identical in the visible region.

Both complexes are emissive in acetonitrile solutions at room temperature (Table 1 and Figure 3). In air, emission spectra exhibit broad featureless bands indicative of a ^{3}MLCT/^{3}LLCT state. The emission maxima for both complexes are around 672-675 nm again showing the photophysics to be independent of the triazole substituent. Analysis of the luminescence lifetimes reveals three component processes with the longest component reaching 268 and 335 ns timescales for **1**$^+$ and **2**$^+$ respectively.

Preliminary emission spectra recorded for the hexafluorophosphate salts in dichloromethane resulted in emission maxima at 632 nm (ESI), significantly blue-shifted relative to the acetonitrile spectra. This blue shift upon increasing solvent polarity confirms the large ^{3}MLCT character for the dominant feature in these spectra.

Upon degassing acetonitrile solutions of the chloride salts the lifetimes are elongated with the longest component being on the order of a microsecond and the quantum yields increase to 0.21 % and 0.43 % for **1**$^+$ and **2**$^+$ respectively. These are relatively low quantum yields for emission and in some cases incorporation of triazole donors has been observed to lead to reduced emission intensity, possibly through increased solvent interactions.[34-36] What is noticeable is that under degassed conditions the emission spectra exhibit features that indicate some structured emission underlying the broad largely featureless band observed in air. This is suggestive of additional emission with significant ^{3}LC character and may account for the multicomponent lifetime. The long lifetimes accompanying the relatively low quantum yields in these complexes may derive from long-lived dark states which are non-emissive but with which the observed emissive states may be in equilibrium. Very similar effects have been observed before in Re^I(dppz) complexes.[39, 40] As emission from both complexes is significantly quenched in aqueous solution, reliable quantum yields could not be obtained.

Computational modelling of the complexes was achieved through optimisation of the geometry of the cation using density functional theory (DFT) calculations. As the triazole N1-substituent has little effect on the photophysical properties

the analogue of $\mathbf{1}^+$ and $\mathbf{2}^+$ bearing simple methyl substituents was investigated. Calculations at the optimised ground state geometry reveal that the highest occupied molecular orbital (HOMO, Figure 4) exhibits the expected localisation at the metal centre with additional contributions from the metalated aryl ring π-system. The lowest unoccupied molecular orbital (LUMO) is localised on the dppz ligand in agreement with results obtained for comparable complexes.

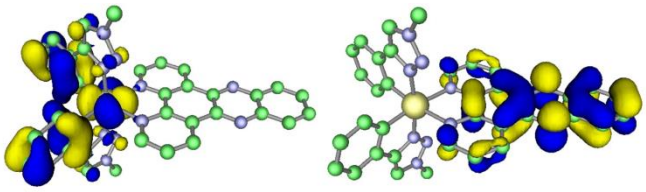

Figure 4. Plots of the HOMO (left) and LUMO (right) orbitals for $\mathbf{1}^+/\mathbf{2}^+$ from DFT calculations.

Biological Studies

DNA Titrations.

The two new complexes incorporate a Ir^{III}(dppz) unit, a moiety that is known to interact with DNA through intercalation. Since binding to DNA often affects the optical absorption and emission properties of such complexes the interaction of complexes $\mathbf{1}^+$ and $\mathbf{2}^+$ with calf-thymus DNA (CT-DNA) was investigated using optical spectroscopy.

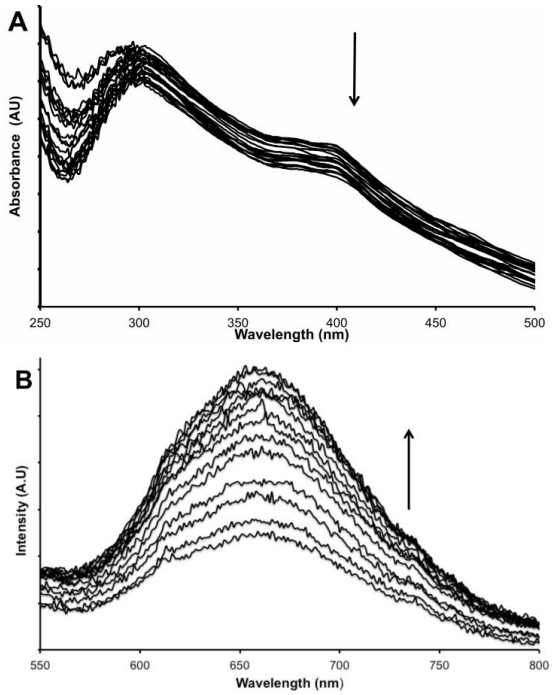

Figure 5 Examples of optical titrations: **(A)** Details of changes in the UV-Visible absorption spectrum of $\mathbf{1}^+$ on addition of duplex DNA **(B)** Increase in emission intensity of complex $\mathbf{1}^+$ on addition of DNA. Conditions: 5 mM Tris buffer, 25 mM NaCl pH 7.4 at 25 °C; 1 μL incremental additions of a 16.4 μM CT-DNA solution.

UV visible absorption studies. Both $\mathbf{1}^+$ and $\mathbf{2}^+$ show distinctive spectral changes on addition of duplex DNA with the UV-Visible absorption spectra of the complexes displaying hypochromicity in their low energy bands (Figure 5A). These changes are typically seen when a solvated complex moves into the more hydrophobic environment of a DNA helix,[27] and are indicative of an interaction between the extended aromatic system of the complex and stacked bases within the duplex.

Luminescence studies. As is the case with most M(dppz) complexes, DNA-induced changes in the emission properties of both complexes could also be used as a spectroscopic tool for studying their interactions with DNA.[2] 1 μL incremental addition of 16.4 μM CT-DNA to buffered solutions of $\mathbf{1}^+$ and $\mathbf{2}^+$ complexes leads to concomitant increase in emission intensity (Figure 5B). Although these changes are not as profound as those observed for the original DNA 'light switch' $[Ru(bpy)_2(dppz)]^{2+}$ they are similar to those that occur with other Ir^{III}(dppz) systems incorporating cyclometalated ancillary ligands[3], suggesting that emission is from a state with significant $Ir^{III}\rightarrow$dppz ^{3}MLCT character.

Using the DNA-induced luminescence changes estimates of binding parameters for the interaction of the complexes with CT-DNA were calculated using the non-cooperative McGhee Von Hippel model for fitting non-linear Scatchard plots (Table 2). As expected from previously discussed electrostatic considerations, the estimated affinities are notably lower than those observed for dicationic M(dppz) systems but they are still appreciable and are typical of those reported for other monocationic dppz complexes[2, 41, 42] It had been hoped that the introduction of the benzyl groups in $\mathbf{1}^+$ might provide additional intercalative π-stacking to stabilise the DNA adduct. Unfortunately, from the data in Table 2 the binding constant for the benzyl substituted complex is inferior to its propyl substituted analogue; it seems the larger benzyl groups act to sterically hinder DNA binding relative to $\mathbf{2}^+$. However, given that the complexes do nevertheless interact with a representative biomolecule, their cellular uptake properties were then investigated.

Table 2. Estimated duplex DNA binding parameters for complexes $\mathbf{1}^+$ and $\mathbf{2}^+$.[a]

Complex	K (M^{-1})	n (bp)[a]
$\mathbf{1}^+$	2.38×10^4	2.7
$\mathbf{2}^+$	5.37×10^4	9.5

a Data fitted with $R^2 \geq 0.95$.

Cellular uptake and imaging studies

Uptake experiments were performed in two common cell lines, the breast cancer cell line MCF7 and the ovarian cancer line A2780. When either was exposed to 50 μM solutions of both complexes over a 24 hour period, wide field luminescence microscopy images revealed that both complexes displayed moderate cellular uptake. Furthermore, whilst the complexes bind DNA in cell-free conditions the images indicated that both complexes are largely localized in the cytosol (Fig 6). Localization within the cytosol as opposed to the nucleus is often due to a subtle balance of hydrophobicity and lipophobicity[43] and in this case it seems the lipophilicity of the monocations is driving the observed preference in accumulation.

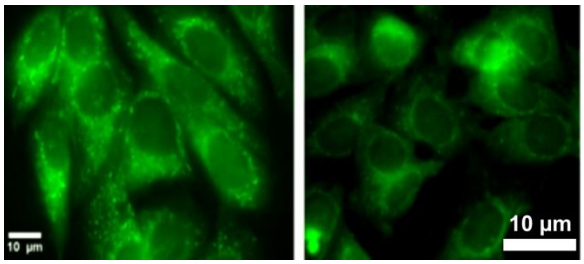

Figure 6 Cellular uptake of $\mathbf{1}^+$ (left) and $\mathbf{2}^+$ (right) in MCF7 cells following 24 hours exposure to 50 µM solutions (Pseudo colouring has been employed in all the images)

The cytotoxicity of the complexes, assessed through IC_{50} values obtained using the well-established MTT assay, are relatively low with MCF7 cells (>200 µM); however, the cytotoxicity towards A2780 is higher with IC_{50} values of 59 µM ($\mathbf{1}^+$) and 151 µM ($\mathbf{2}^+$) respectively. It was noted that A2780 cells treated with the complexes appeared to be particularly brightly stained. Consequently more detailed studies on the uptake and localization of the two complexes were carried out.

To accurately determine the extent of intracellular localization, ICP-MS experiments were carried out on both MCF7 and A2780 cells under identical conditions. Interestingly, in both cell lines, $\mathbf{1}^+$ is taken up at higher concentrations than $\mathbf{2}^+$; by a factor of 3 in A2780 and a factor of 11 in MCF-7. It should be noted that complex $\mathbf{1}^+$ contains more lipophilic ligands which may be a factor in terms of diffusion across the cell membrane (Figure 7). ICP-MS measurements were taken at 1 hour and 24 hours after exposure to the complexes and these time points show there is steady accumulation over the 24 hour time period, indicative of passive diffusion taking place across the membrane. A comparison of the data also shows that uptake of both complexes is significantly higher in A2780 cells relative to MCF7 cells. These data reflect the observed trend in IC_{50} figures, illustrating how cytotoxicity effects are often, at least partly, a function of cell internalisation.

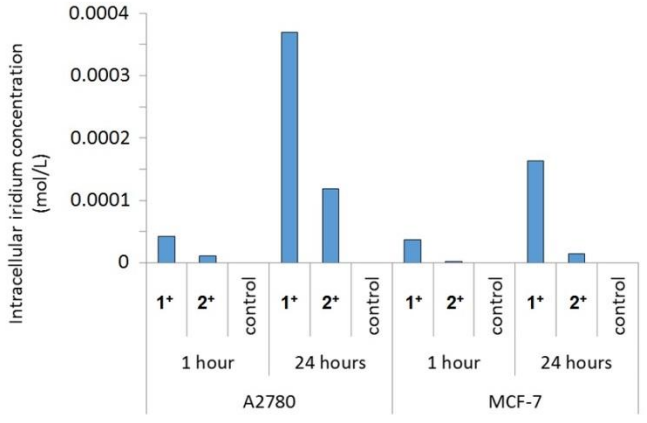

Cell Line	[$\mathbf{1}^+$] / µM (24 h)	[$\mathbf{2}^+$] / µM (24 h)
A2780	369	119
MCF-7	163	14

Figure 7. ICP-MS data summarizing cellular uptake of both the complexes in A2780 and MC7 cells

The microscope images of cells stained by $\mathbf{1}^+$ and $\mathbf{2}^+$ show punctate emission from the cytosol suggesting specific localization. To explore this issue further, intracellular tracking experiments were performed. However before these could begin, the spectral characteristics of both the complexes were considered so that suitable co-staining dyes for tracking experiments could be selected.

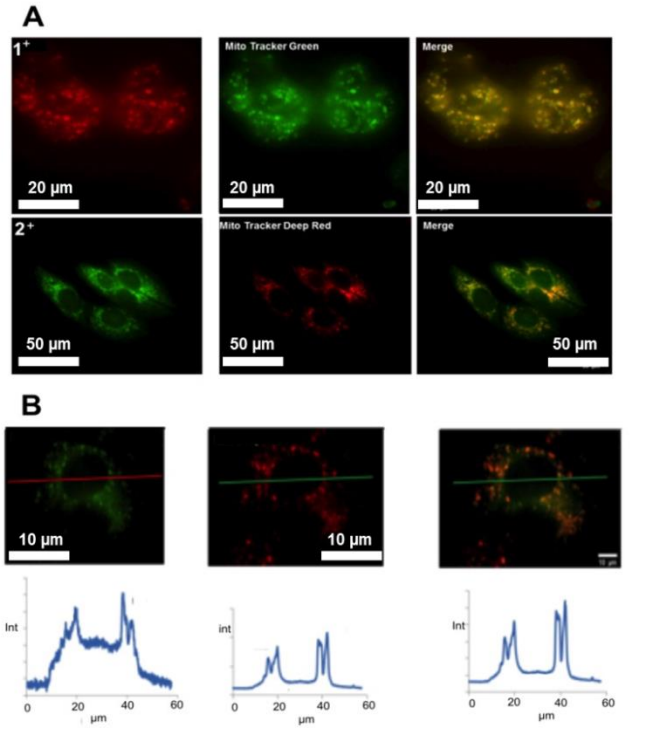

Figure 8. (A): Co-localisation studies of complex $\mathbf{1}^+$ with MTG (Top) and complex $\mathbf{2}^+$ with MTDR (Bottom) in A2780 cells using wide field microscopy. **(B):** Detailed co-localisation data for $\mathbf{1}^+$(left), MTDR (middle) and merged image (right). Luminescence intensity vs. distance plots along the marked lines are shown at the bottom of the figure. Pseudo colouring has been employed in all the images.

Since lipophilic cations often accumulate in mitochondria,[44, 45] colocalisation with commercial mitochondrial probes was investigated. When excited at 470 nm, both complexes showed emission in the RFP region (570 nm to 620 nm). Therefore Mito Tracker Green, MTG, was chosen for initial intracellular tracking experiments as this shows emission in the GFP channel. Although MTG is also excited at 470 nm its emission output is observed at 500 nm to 540 nm. To rule out the possibility of cross talk between adjacent channels, experiments with Mito Tracker Deep Red, MTDR, were also carried out. MTDR is excited at 640 nm and emits between 660 nm and 700 nm (Cy5 region). As shown in Figure 8, these experiments revealed a very strong correlation between the intracellular emission localities of the complexes with MTG and MTDR. Intensity versus distance plots as shown in Figure 8 also confirmed a near perfect colocalisation with mitochondria. Indeed calculated Pearson and Mander coefficients for both $\mathbf{1}^+$ and $\mathbf{2}^+$ indicate ≥90% colocalisation with MTDR (Table 3). Whilst the complex has been shown to bind to DNA leading to luminescent enhancement it is possible that additional luminescent enhancements might occur

through interactions with other biomolecules including proteins.

Table 3. Co-localisation coefficients for complexes $\mathbf{1}^+$ and $\mathbf{2}^+$ with MTDR

Compound	Pearson's Coefficient	Mander's M1	Mander's M2
$\mathbf{1}^+$	0.903	0.999	0.925
$\mathbf{2}^+$	0.885	0.986	0.863

Conclusion

Two new iridium(III) complexes bearing a dppz DNA-intercalating ligand along with cyclometalated phenyltriazole ligands have been reported. The complexes exhibit a luminescence "switch on" effect upon binding with DNA with reasonable binding coefficients for monocationic complexes. Cellular uptake experiments show that they localize within the cytosol. The complexes are shown to localize at the mitochondria with relatively high Pearson coefficients (> 0.89), demonstrating the specificity of the probes towards mitochondria. Given the wide range of triazole-based ligands available and the tuneable photophysical properties of Ir^{III} moieties, these new complexes open up new avenues for the development of novel, highly functionalisable, iridium(III) DNA imaging probes and phototherapeutics.

Experimental Section

General methods

Chemicals were purchased from Sigma-Aldrich and Acros Organics. Iridium(III) chloride was purchased from Precious Metal Online (Monash, Australia) and used as received. All complexation reactions were carried out under nitrogen. Dipyrido[3,2-a:2',3'-c]phenazine (dppz)[46] and aryl triazole ligand precursors[47] were prepared according to literature procedures. ^{1}H NMR and ^{13}C NMR spectra were recorded on a Bruker Avance 400 MHz instrument. Mass spectrometry data were collected on a Bruker Micro Q-TOF instrument. UV-Visible absorption spectra were recorded on a Varian Cary 300 spectrophotometer and corrected emission spectra were recorded on a Horiba Fluoromax-4 spectrofluorometer. Luminescence lifetime measurements were carried out using an Edinburgh Instruments Mini-Tau spectrometer.

Computational methods

DFT calculations were carried out using the NWChem 6.3 software package[48], B3LYP hybrid functional (20% Hartree–Fock) method has been used for calculations[49], Stuttgart relativistic small core ECP[50] for transition metals and 6-311G* basis sets for all other atoms. Molecular geometries and molecular orbitals pictures were realised using the ccp1 graphical software. For all the studied complexes, the ground state geometries were first optimized and molecular orbital energies determined. The COSMO solvation model, built into NWChem software, was used in obtaining the electronic spectra and molecular orbital energy levels and plots.

Synthesis of $[Ir(ptz^{Bn})_2(dppz)](PF_6)_2$ (1.PF_6)

1-benzyl-4-(phenyl)-1,2,3-triazole (267 mg, 1.134 mmol) was added to a 3:1 (v/v) solution of ethoxyethanol and water (18 mL). Iridium chloride trihydrate (200 mg, 0.567 mmol) was then added and the solution left to stir at 110°C overnight. The solution was then allowed to cool and the crude biscyclometalated dimer filtered under vacuum and purified by column chromatography (2% methanol in DCM). The resulting dimer (100 mg), together with 2 equivalents of dppz (40 mg), was refluxed in 25 ml 1:2 (v/v) methanol/dichloromethane for 12 hours. After cooling, the solvent was removed and the product purified by column chromatography on SiO_2 with a 7:1:0.5 solution of acetonitrile, saturated aqueous potassium nitrate and water respectively. The orange fraction was dried under vacuum, redissolved in acetonitrile and filtered. The solution was dried again and the solid was dissolved in methanol and stirred with an excess of NH_4PF_6 for 3 hours. The product was precipitated through addition of ether, washed with water and again ether. (Yield 88 mg, 57%)

^{1}H NMR (400 MHz, CD_3CN) δ: 9.29 (dd, *J* = 1.3, 8.2 Hz, 2H); 8.44 (dd, *J* = 1.4, 5.2 Hz, 2H); 8.17 (dd, *J* = 3.4, 6.4 Hz, 2H); 8.15 (s, 2H); 8.00 (dd, *J* = 3.4, 6.6 Hz, 2H); 7.74 (dd, *J* = 5.2, 8.2 Hz, 2H); 7.57 (dd, *J* = 1.0, 7.6 Hz, 2H); 7.15-7.02 (m, 12H); 6.91 (td, *J* = 1.4, 7.5 Hz, 2H); 6.36 (d, *J* = 7.1 Hz, 2H); 5.38 (d, *J* = 15.1 Hz, 2H); 5.34 (d, *J* = 15.1 Hz, 2H).

^{13}C NMR (400 MHz, CD_3CN) δ: 157.18, 152.99, 150.15, 145.08, 142.41, 139.22, 135.91, 134.62, 134.27, 132.59, 132.41, 129.94, 129.47, 128.84, 128.58, 128.41, 127.9, 127.31, 122.98, 122.63, 120.11, 55.22

HRMS (ESI) calcd: $C_{48}H_{34}IrN_{10}^+$ 943.2597, found: 943.2590 (M^+)

Synthesis of $[Ir(ptz^{Pr})_2(dppz)](PF_6)_2$ (2.PF_6)

The synthetic procedure was the same as that for **1**.PF_6, except that 4-phenyl-1-propyl-1,2,3-triazole (212 mg) was used in place of 1-benzyl-4-(phenyl)-1,2,3-triazole. (Yield 65 mg, 64%)

^{1}H NMR (400 MHz, CD_3OD) δ: 9.46 (dd, *J* = 1.2, 8.2 Hz, 2H); 8.55 (dd, *J* = 1.3, 5.1 Hz, 2H); 8.40 (s, 2H); 8.17 (dd, *J* = 3.4, 6.5 Hz, 2H); 7.96 (dd, *J* = 3.4, 6.6 Hz, 2H); 7.89 (dd, *J* = 5.3, 8.7 Hz, 2H); 7.6 (d, *J* = 7.5 Hz, 2H); 7.02 (td, *J* = 1.0, 7.7 Hz, 2H); 6.90 (td, *J* = 1.2, 7.5 Hz, 2H); 6.37 (d, *J* = 7.4 Hz, 2H); 4.22 (t, *J* = 7.0 Hz, 4H); 1.80 (m, 4H); 0.77 (t, *J* = 7.4 Hz, 6H).

^{13}C NMR (400 MHz, CD_3OD) δ: 155.89, 151.49, 148.89, 143.56, 141.11, 137.79, 134.5, 133.18, 130.97, 130.62, 128.68, 127.88, 126.68, 125.59, 121.21, 120.78, 118.1, 51.74, 21.59, 8.16.

HRMS (ESI) calcd m/z: $C_{40}H_{34}IrN_{10}^+$ 847.2597, found: 847.2581 (M^+)

Counter ion metathesis

Both **1**.PF_6 and **2**.PF_6 complexes, after their isolation, underwent an anion metathesis. The corresponding solids were stirred in methanol with Amberlite IRA-400 chloride form ion-exchange resin (complex:resin 1:5 w/w) at room temperature for four hours. The suspensions were filtered, the solvent was removed under vacuum and the products

recrystallised from acetonitrile and ether, quantitatively yielding the salts **1**.Cl and **2**.Cl. Successful removal of the hexafluorophosphate anion was confirmed by the absence of signals in $^{31}P\{^{1}H\}$ and $^{19}F\{^{1}H\}$ NMR spectra.

DNA titration Experiments

Reagents:

Reagents used for carrying out DNA titration experiments include CT-DNA (Aldrich), tris buffer (5 mM Tris, 25 mM NaCl) (in-house).

UV-Visible absorption DNA titration:

UV-Visible spectra were recorded on a thermally regulated Varian-Carey Bio-300 UV-Visible spectrometer, using quartz cells of 10 mm path length at 25°C. Spectra were baseline corrected using Cary Win UV software and were diluted accordingly to give readings between 0.2 and 1.0 absorbance units.

Method:

3 ml of buffer solution was loaded into a 10 mm path length cuvette and allowed to equilibrate inside the spectrometer before a baseline reading was taken. A 50 µM solution of complex ($\mathbf{1}^+$ or $\mathbf{2}^+$) was prepared using the buffer and the plain buffer was replaced with this to titrate with the CT-DNA. After equilibration the spectrum was recorded between 200-600 nm. 1 µL of a concentrated stock solution of CT-DNA (16.4 mM) was added to the cuvette and mixed vigorously with a pipette to ensure homogeneity. The spectrum was recorded after leaving the sample to equilibrate for 3 minutes eliminating the air bubbles completely. This procedure was continued until the absorbance became constant or the increase of CT-DNA concentration only caused small changes in the absorption spectra.

Luminescence DNA titration:

Luminescence spectra were recorded on a thermally regulated Jobin-Yvon FluoroMax-3 spectrophotometer operating in luminescence wavelength scan mode at 25°C, with 5 nm excitation and emission slit widths.

Method:

3 ml of buffer was loaded into a 10 mm path length cuvette and allowed to equilibrate inside the spectrometer before a baseline reading was taken. A 50 µM solution ($\mathbf{1}^+$ or $\mathbf{2}^+$) was prepared using the buffer and the plain buffer was replaced with this to titrate with the CT-DNA. After equilibration the spectrum was recorded between 500-800 nm. 2.5 µL of a concentrated stock solution of CT-DNA (16.4 mM) was added to the cuvette and mixed vigorously with a pipette to ensure homogeneity. The spectrum was recorded after leaving the sample to equilibrate for 3 minutes eliminating the air bubbles completely. The emission spectrum was recorded, showing an increase in emission on incremental addition of CT-DNA. The procedure was continued until saturation.

Microscopy Experiments:

Reagents:

Reagents used for the Microscopy and Tissue culture experiments include, RPMI 1640 with L-glucose and sodium bicarbonate (Aldrich), Phosphate Buffer Saline (PBS) (Aldrich), foetal bovine serum (Aldrich), penicillin streptomycin (Aldrich), 4% paraformaldehyde (PFA) (Aldrich), Vectashield h-1000 (mounting agent) (Aldrich), 50 mM ammonium chloride (Aldrich), Mito Tracker Green (Aldrich), Mito Tracker Deep Red (Aldrich). Other items required for sample preparation include 26 mm X 76 mm Microscopy glass slides, 22 mm X 22 mm (170 ± 5 µm square Cover glasses (Thor labs.)

Instrument Details:

Wide Field Fluorescence Microscopy was carried out by using a Nikon Dual cam Wide Field Fluorescence Microscope. The details of the Microscope include: Excitation source: SpectraX LED excitation (395 nm, 440 nm, 470 nm, 508 nm, 561 nm, 640 nm); Emission Filter sets: Single filters for DAPI, GFP, RFP, Cy5; Quad filter for DAPI/GFP/RFP/Cy5 with matching emission filter wheel; Detector set: Dual Andor Zyla sCMOS, 2560 x 2160; 6.5µm pixels and inbuilt NIS software was employed for Wide Field Deconvolution.

Method:

The Wide Field Fluorescence Microscopy involves collection of greater quantity of light (including out of focus light) compared to the confocal microscopy technique which involves loss of more than 30% of light as out of focus light is discarded during image acquisition as it is a pointillistic technique[17]. The Wide field Microscopy technique involves improvement in resolution only after post processing the Z-stacks acquired. Processing of acquired data was achieved by using Fiji software.

Deconvolution Wide Field Microscopy:

The Deconvolution procedure involves the processing of the raw Wide Field images obtained from the Nikon Dual cam Wide Field Microscope. This image processing is carried out by using the NIS software. Deconvolution is a computationally intensive image processing technique which helps in improving the contrast and Axial resolution post acquisition of the images from 400 nm to 350 nm. During the Deconvolution procedure the raw Wide Field images are processed by removing the out of focus blur from stack of acquired images called Z-Stack.

Cellular uptake (Single colour imaging):

The complexes $\mathbf{1}^+$ and $\mathbf{2}^+$ were excited at 470 nm and the emission was collected between 570 nm to 620 nm (RFP channel of Dual cam Nikon Wide Field Fluorescence Microscope). The Wide Field imaging conditions employed for the cellular uptake studies of the A2780 and MCF7 cells is shown Fig. 6 and Fig. S1 and in the Supporting Information videos (CC203-204-WF-Video-1, CC203-204-WF-Video-2 and CC203-204-WF-Video-4). The Wide Field Microscopy conditions maintained include: Thickness of the Z stack (Sections 40 to 100); Section spacing (0.250 to 0.500); Thickness of the sample (8 to 15).

Colocalisation (Multi colour imaging):

The complexes $\mathbf{1}^+$ and $\mathbf{2}^+$ was excited at 470 nm and the emission was collected between 570 nm to 620 nm (RFP channel), Mito Tracker Green was excited at 470 nm and the emission was collected between 500 nm to 530 nm (GFP channel), Mito Tracker Red Deep Red was excited at 640 nm and collected between 650 nm to 700 nm (Cy5 channel). The colocalisation of $\mathbf{1}^+$ and $\mathbf{2}^+$ with Mito Tracker Green and the

colocalisation of $\mathbf{1}^+$ and $\mathbf{2}^+$ with Mito Tracker Deep Red is shown in Fig. 8 and the colocalisation of $\mathbf{1}^+$ was shown in the Supporting Information video CC203-204-WF-Video-3. The colocalisation experiments were carried out using the same microscopy conditions as mentioned above for the cellular uptake experiments.

Tissue Culture Experiments:

Cellular Uptake studies for $\mathbf{1}^+$ and $\mathbf{2}^+$:

A2780 or MCF7 cells were seeded on cover slips (22 mm X 22 mm, 170 ± 5 µm square cover glasses) placed in six well plates in RPMI culture medium containing (10% FBS and 1% penicillin streptomycin) for 24 hours at 37°C, 5% CO_2. After 24 hours when 70% confluency was achieved the cells were washed with RPMI culture medium then the cells were treated with $\mathbf{1}^+$ or $\mathbf{2}^+$ (50 µM or 100 µM) for 24 hours[51]. Cells were then washed thrice with culture medium. After that cells were washed again with Phosphate Buffer Saline (2X PBS). After carrying out the live cell uptake of $\mathbf{1}^+$ or $\mathbf{2}^+$ the cells were then fixed with 4% PFA for 15 minutes and then washed thrice with PBS and two times with 50 mM ammonium chloride solution and then the cover slips were mounted using mounting medium (Vectashield h-1000).The Coverslips were then sealed using nail varnish and the sample were then imaged by Wide Field Fluorescence Microscopy using the Dual cam Nikon.

Colocalisation studies for $\mathbf{1}^+$ and $\mathbf{2}^+$:

The colocalisation studies of $\mathbf{1}^+$ and $\mathbf{2}^+$ was carried out by using Mito Tracker Green and Mito Tracker Red. A2780 cells were seeded on cover slips (22 mm X 22 mm, 170 ± 5 µm square Cover glasses) placed in six well plates in RPMI culture medium containing (10% FBS and 1% penicillin streptomycin) for 24 hours[51] at 37°C, 5% CO_2. After 24 hours when 70% confluency was achieved the cells were washed with RPMI culture medium then the cells were treated with 1 µM (Mito Tracker Green or Mito Tracker Deep Red) for 30 minutes and washed with 2X RPMI culture media and then treated with 50 µM $\mathbf{1}^+$ or $\mathbf{2}^+$ for 24 hours. Cells were then washed thrice with culture medium. After that cells were washed again with Phosphate Buffer Saline (2X PBS). After carrying out the live cell uptake of $\mathbf{1}^+$ or $\mathbf{2}^+$ the cells were then fixed with 4% PFA for 15 minutes and then washed thrice with PBS and two times with 50 mM ammonium chloride solution and then the cover slips were mounted using mounting medium (Vectashield h-1000). The coverslips were then sealed using nail varnish and the sample were then imaged by Wide Field Fluorescence Microscopy using the Dual cam Nikon.

ICP-MS:

Cell cultures were grown on 60 mm dishes at a seeding density of 5 x10^5 cells per dish and incubated for 24 h. Cells were then treated with the complex (solubilised in and maintained at 10% PBS/H_2O: 90% medium throughout all solutions) at the stated concentration and incubated for 24 h. All complex solution (or control medium) was removed, cells washed and 200 µL serum free medium added. Cells were detached by scraping and transferred to a falcon tube, where 20 µL of each sample was removed for cell counting. Each sample was transferred to a glass sample tube, 1 ml concentrated HNO_3 added, heated to 60°C overnight and then diluted to 5 ml total volume with ultrapure Milli-Q H_2O before analysis of iridium content by inductively coupled plasma mass spectrometry (ICP-MS). Using the obtained iridium concentration, the sample volume, number of cells per sample and the assumption of a cell volume of 2 x10^{-12} L an estimate of intracellular concentration (mol L^{-1}) could be deduced.

Cytotoxicity:

Cells were maintained in RPMI 1640 medium supplemented with 10% FBS, 100 mg ml^{-1} streptomycin, 100 mg ml^{-1} penicillin, and 2 mM glutamine at 37°C in a humidified atmosphere containing 5% CO_2. Experimental cultures were grown on 48 well plates at a seeding density of 5 x 10^4 cells per well and incubated for 24 h. The cells were then treated with complex (solubilised in DMSO and PBS and maintained at a final concentration of 9.99% PBS and 0.01% DMSO throughout all solutions) of a 1 – 200 µM concentration range, in triplicate, and incubated for 48 h. The culture media was removed and cells incubated with MTT (0.5 mg ml^{-1} dissolved in PBS) for 30 – 40 min. The MTT was removed and formazan product eluted using 120 µl/well acidified isopropanol, 100 µl of which was transferred to a 96 well plate for the absorbance to be quantified by spectrophotometer (540 nm, referenced at 640 nm). An average absorbance for each concentration was calculated and cell viability was determined as a percentage of the untreated negative control wells (0.1% DMSO:9.99% PBS:90% medium, average of triplicate). Data were plotted in a graph of concentration against cell viability to produce a curve from which the IC_{50} value could be derived by interpolation.

Acknowledgements

The authors would like to thank the University of Huddersfield (A.S., C.C.) and the University of Sheffield (S.S., P.J.J., D.R., C.G.W.S and J.A.T) for supporting this work. A.S. also thanks the Foundation Blanceflor Boncompagni-Ludovisi for financial support. As a member of the UK Materials Chemistry Consortium PIPE also thanks the EPRSC and the UK HPC national resource, Archer (EP/L000202), as well as the Huddersfield High Performance Computing Research Group for computational facilities utilised in this work. S.S and J.A.T are grateful to the Imagine Imaging Cohort 2022 Futures initiative of the University of Sheffield and would like to thank the MRC (MR/K015753/1) funding for the microscopy facilities.

Conflicts of interest

There are no conflicts to declare.

References

1. E. Baggaley, J. A. Weinstein and J. A. G. Williams, *Coordination Chemistry Reviews*, 2012, **256**, 1762-1785.
2. M. R. Gill and J. A. Thomas, *Chemical Society Reviews*, 2012, **41**, 3179-3192.
3. K. K. W. Lo, *Accounts of Chemical Research*, 2015, **48**, 2985-2995.

4. K. K. W. Lo, S. P. Y. Li and K. Y. Zhang, *New Journal of Chemistry*, 2011, **35**, 265-287.
5. K. K. W. Lo, M. W. Louie and K. Y. Zhang, *Coordination Chemistry Reviews*, 2010, **254**, 2603-2622.
6. Q. Zhao, C. Huang and F. Li, *Chemical Society Reviews*, 2011, **40**, 2508-2524.
7. V. Fernández-Moreira, F. L. Thorp-Greenwood and M. P. Coogan, *Chemical Communications*, 2010, **46**, 186-202.
8. C. P. Montgomery, B. S. Murray, E. J. New, R. Pal and D. Parker, *Accounts of Chemical Research*, 2009, **42**, 925-937.
9. J. A. Thomas, *Chemical Society Reviews*, 2015, **44**, 4494-4500.
10. A. E. Friedman, J. K. Barton, J. C. Chambron, J. P. Sauvage, N. J. Turro and J. K. Barton, *Journal of the American Chemical Society*, 1990, **112**, 4960-4962.
11. R. M. Hartshorn and J. K. Barton, *Journal of the American Chemical Society*, 1992, **114**, 5919-5925.
12. G. Li, L. Sun, L. Ji and H. Chao, *Dalton Transactions*, 2016, **45**, 13261-13276.
13. Z. Chen, K. Y. Zhang, X. Tong, Y. Liu, C. Hu, S. Liu, Q. Yu, Q. Zhao and W. Huang, *Advanced Functional Materials*, 2016, **26**, 4386-4396.
14. S. Liu, Y. Zhang, H. Liang, Z. Chen, Z. Liu and Q. Zhao, *Optics Express*, 2016, **24**, 15757-15764.
15. W. Lv, Z. Zhang, K. Y. Zhang, H. Yang, S. Liu, A. Xu, S. Guo, Q. Zhao and W. Huang, *Angewandte Chemie - International Edition*, 2016, **55**, 9947-9951.
16. S. Liu, N. Zhou, Z. Chen, H. Wei, Y. Zhu, S. Guo and Q. Zhao, *Optics Letters*, 2017, **42**, 13-16.
17. K. Y. Zhang, Q. Yu, H. Wei, S. Liu, Q. Zhao and W. Huang, *Chemical Reviews*, 2018.
18. H. Z. He, K. H. Leung, W. Wang, D. S. H. Chan, C. H. Leung and D. L. Ma, *Chemical Communications*, 2014, **50**, 5313-5315.
19. F. Lu and T. Nabeshima, *Dalton Transactions*, 2014, **43**, 9529-9536.
20. C. Jin, J. Liu, Y. Chen, L. Zeng, R. Guan, C. Ouyang, L. Ji and H. Chao, *Chemistry - A European Journal*, 2015, **21**, 12000-12010.
21. T. S. M. Tang, K. K. Leung, M. W. Louie, H. W. Liu, S. H. Cheng and K. K. W. Lo, *Dalton Transactions*, 2015, **44**, 4945-4956.
22. K. Y. Zhang, H. W. Liu, M. C. Tang, A. W. T. Choi, N. Zhu, X. G. Wei, K. C. Lau and K. K. W. Lo, *Inorganic Chemistry*, 2015, **54**, 6582-6593.
23. L. L. Sun, Y. Chen, S. Kuang, G. Y. Li, R. L. Guan, J. P. Liu, L. N. Ji and H. Chao, *Chem.-Eur. J.*, 2016, **22**, 8955-8965.
24. R. R. Ye, C. P. Tan, L. N. Ji and Z. W. Mao, *Dalton Transactions*, 2016, **45**, 13042-13051.
25. Y. Liu, P. Zhang, X. Fang, G. Wu, S. Chen, Z. Zhang, H. Chao, W. Tan and L. Xu, *Dalton Transactions*, 2017, **46**, 4777-4785.
26. J. R. Shewring, A. J. Cankut, L. K. McKenzie, B. J. Crowston, S. W. Botchway, J. A. Weinstein, E. Edwards and M. D. Ward, *Inorganic Chemistry*, 2017, **56**, 15259-15270.
27. S. Stimpson, D. R. Jenkinson, A. Sadler, M. Latham, A. Wragg, A. J. H. M. Meijer and J. A. Thomas, *Angewandte Chemie - International Edition*, 2015, **54**, 3000-3003.
28. Y. M. Chen, A. G. Zhang, Y. J. Liu and K. Z. Wang, *Journal of Organometallic Chemistry*, 2011, **696**, 1716-1722.
29. Y. M. Chen, A. G. Zhang and K. Z. Wang, *Applied Organometallic Chemistry*, 2011, **25**, 521-529.
30. K. K. W. Lo, C. K. Chung and N. Zhu, *Chemistry - A European Journal*, 2006, **12**, 1500-1512.
31. F. Shao, B. Elias, W. Lu and J. K. Barton, *Inorganic Chemistry*, 2007, **46**, 10187-10199.
32. R. A. Smith, E. C. Stokes, E. E. Langdon-Jones, J. A. Platts, B. M. Kariuki, A. J. Hallett and S. J. A. Pope, *Dalton Transactions*, 2013, **42**, 10347-10357.
33. S. K. Tripathy, U. De, N. Dehury, P. Laha, M. K. Panda, H. S. Kim and S. Patra, *Dalton Transactions*, 2016, **45**, 15122-15136.
34. J. D. Crowley and D. A. McMorran, *Top. Heterocycl. Chem.*, 2012, **28**, 31-83.
35. P. A. Scattergood and P. I. P. Elliott, *Dalton Transactions*, 2017, **46**, 16343-16356.
36. P. A. Scattergood, A. Sinopoli and P. I. P. Elliott, *Coordination Chemistry Reviews*, 2017, **350**, 136-154.
37. A. B. Tamayo, S. Garon, T. Sajoto, P. I. Djurovich, I. M. Tsyba, R. Bau and M. E. Thompson, *Inorg. Chem.*, 2005, **44**, 8723.
38. C.-H. Yang, S.-W. Li, Y. Chi, Y.-M. Cheng, Y.-S. Yeh, P.-T. Chou, G.-H. Lee, C.-H. Wang and C.-F. Shu, *Inorg. Chem.*, 2005, **44**, 7770.
39. J. Dyer, W. J. Blau, C. G. Coates, C. M. Creely, J. D. Gavey, M. W. George, D. C. Grills, S. Hudson, J. M. Kelly, P. Matousek, J. J. McGarvey, J. McMaster, A. W. Parker, M. Towrie and J. A. Weinstein, *Photochemical and Photobiological Sciences*, 2003, **2**, 542-554.
40. H. D. Stoeffler, N. B. Thornton, S. L. Temkin and K. S. Schanze, *Journal of the American Chemical Society*, 1995, **117**, 7119-7128.
41. V. G. González, University of Sheffield, 2006.
42. C. Metcalfe, H. Adams, I. Haq and J. A. Thomas, *Chemical Communications*, 2003, **9**, 1152-1153.
43. S. Trapp and R. W. Horobin, *European Biophysics Journal*, 2005, **34**, 959-966.
44. M. P. Murphy, *Biochimica et Biophysica Acta - Bioenergetics*, 2008, **1777**, 1028-1031.
45. H. K. Saeed, P. J. Jarman, S. Archer, S. Sreedharan, I. Q. Saeed, L. K. McKenzie, J. A. Weinstein, N. J. Buurma, C. G. W. Smythe and J. A. Thomas, *Angewandte Chemie - International Edition*, 2017, **56**, 12628-12633.
46. Y. Sun, S. N. Collins, L. E. Joyce and C. Turro, *Inorg. Chem.*, 2010, **49**, 4257.
47. B. S. Uppal, R. K. Booth, N. Ali, C. Lockwood, C. R. Rice and P. I. P. Elliott, *Dalton Transactions*, 2011, **40**, 7610-7616.
48. M. Valiev, E. J. Bylaska, N. Govind, K. Kowalski, T. P. Straatsma, H. J. J. V. Dam, D. Wang, J. Nieplocha, E. Apra, T. L. Windus and W. d. Jong, *Comp. Phys. Commun.*, 2010, **181**, 1477.
49. P. J. Stephens, F. J. Devlin, C. F. Chabalowski and M. J. Frisch, *J. Phys. Chem.*, 1994, **98**, 11623.
50. D. Andrae, U. Haussermann, M. Dolg, H. Stoll and H. Preuss, *Theor. Chim. Acta*, 1990, **77**, 123.
51. Y. Zhou, J. Jia, W. Li, H. Fei and M. Zhou, *Chemical Communications*, 2013, **49**, 3230-3232.